# Colloidal spherocylinders at an interface: Flipper dynamics and bilayer formation

# Colloidal spherocylinders at an interface: flipper dynamics and bilayer formation

T. Li, G. Brandani, D. Marenduzzo, P. S. Clegg
*SUPA, School of Physics and Astronomy, University of Edinburgh, Edinburgh EH9 3FD, United Kingdom*

We study the response of a film of colloidal spherocylinders to compression by combining pressure-area isotherm measurements, microscopy and computer simulations. We find that the behavior of the film depends strongly on the geometry of the particles. For small aspect ratio, a uniform monolayer forms and then buckles. For higher aspect ratio, particles flip to orient perpendicular to the interface; we show that flipping occurs in locations where the nematic ordering is low. Our experiments and simulations further demonstrate that the longest particles rearrange to self assemble a colloidal bilayer, which is stable due to the unique geometry of spherocylinders at an interface.

PACS numbers: 62.20.mq, 64.70.pv, 68.05.Cf

The physics of particle-laden interfaces has been an intense focus of research within physics for some time [1]. These structures are created by dispersing spherical particles close to an interface between two immiscible fluids, such as oil and water. Particles get trapped at the fluid-fluid interfaces because this reduces the energetically costly interfacial area. The free energy gained in doing so is $\sim 10^3 - 10^6\ k_BT$ for a particle of size $\sim 100nm$–$1\mu$m: hence, adsorption on the interface is virtually permanent [2]. This principle is the basis of the stability of so-called "Pickering emulsions", comprised of particle-covered droplets [3]. Once on the interface, colloidal particles can further self-assemble into ordered two-dimensional structures, by virtue of interparticle interactions, often dependent on capillary effects [4].

Recently, the development of new synthesis techniques has allowed advances beyond spherical colloids launching the study of anisotropic micron-sized particles, such as cylinders and ellipsoids [5]. These rod-like building blocks have richer self-assembly potential compared to their spherical counterparts, both in the bulk and when adsorbed onto an interface, due to the packing constraints and the more complex capillary interactions that arise. For example, rod-like particles were shown to produce foams and "Pickering" emulsion with unprecedented stability [6–8].

Previous work on anisotropic particles at fluid-air or fluid-fluid interfaces has focused on cylinders and ellipsoids (with aspect ratio $> 1$). In the absence of an external field, the free energy minimum for an isolated cylinder or ellipsoid on an interface is realised when they lie with their major axes parallel to the interface, so as to cover as much interfacial area as possible. Unlike for spherical particles, the contact line around a cylinder or ellipsoid is no longer flat, since the condition of a constant contact angle $\theta$ at a three-phase contact line, required for the derivation of Young's equation, cannot be met [9–11]. The ensuing distortions to the interface cause capillary interactions between particles, which favour an end-to-end configuration for cylinder pairs, and a side-to-side configuration for ellipsoid pairs [12].

Here, we analyse the self-assembly and compression dynamics of a suspension of colloidal spherocylinders (cylinders capped by hemispherical ends) at a fluid-air interface by combining experiments and simulations. Dynamic compression is a popular practical method to determine the mechanical response of different materials, from hydrogels [13] to the bacterial cell wall [14]. In 2D monolayers, this method allows simultaneous monitoring of the microscopic structure of the system and of the macroscopic surface pressure. Basavaraj *et al.* studied monolayers of monodisperse ellipsoids in this way [15], and observed a series of structural transitions. They also found that, once compression creates a percolating particle network, some of the ellipsoids can flip their long axes to be perpendicular to the interface. This "flipping" process helps relieve some of the compression stress; it was also observed in water-in-oil emulsions stabilised by ellipsoids, when the droplet surface shrinks due to limited coalescence [8].

Our experiments and simulations provide a mechanistic insight into the physics of "flipping", which had, thus far, remained elusive. We find that "flippers" appear only for a range of aspect ratios (ARs), and they do so close to the boundary between nematic domains with conflicting orientations. We also show that spherocylinders (but not ellipsoids) of sufficiently high AR self assemble into a colloidal multilayer under compression. This behavior is due to the unique geometry of spherocylinders, which does not induce any interface deformation when the wetting angle is 90°: in other words, capillary interactions between interfacial particles are absent for ideal spherocylinders [22]. Our multilayer provides an experimental realisation of a self-assembling nematic shell of tunable thickness, a system of interest per se and as a biomimetic analogue of a cytoskeletal actin cortex (with tangential ordering of actin fibers [16]).

We begin by reporting the measured surface pressure-area curves, or Π-A isotherms (Fig. 1). Monolayers were created by spreading the particles at an air-water interface in a Langmuir trough, and a compression study followed. We analyse three ARs: $2.9 \pm 0.3$, $9.2 \pm 0.1$, and $14.8 \pm 0.1$ (see [17] for fabrication details). Silica spheres (0.48 $\mu$m in diameter, inset of Fig. 1) were used

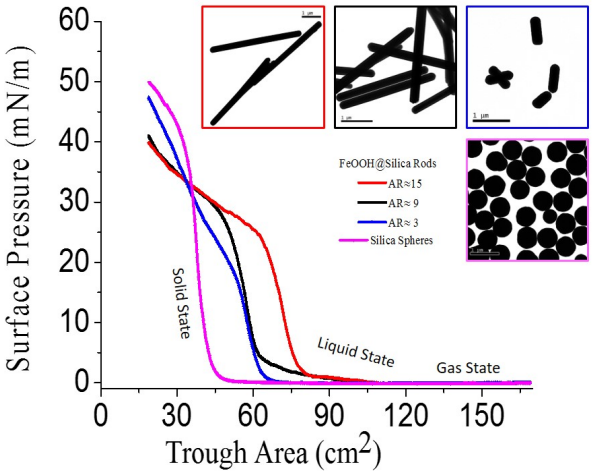


FIG. 1: The Π-A isotherms of monolayers containing silica spheres (pink) and rods with different aspect ratios: AR≃3 (blue), AR≃9 (black), AR≃15 (red). Insets: TEM images of the particles. Scale bars = 1$\mu$m.

as a spherical particle control. The isotherm for spheres shows three possible states (pink line in Fig. 1). There is a gas state, where the surface pressure is close to 0, followed, for smaller trough area, by a solid phase, where particles form a monolayer and the surface pressure increases sharply with density. For very high compaction, particles cannot rearrange within the monolayer, so the interface buckles and the monolayer collapses.

The pressure-area isotherms for anisotropic particles have a more gradual evolution. In particular, in the films containing longer spherocylinders (AR≃9 and 15, black and red curves in Fig. 1), a liquid state appears between the gas and the solid states: this is characterised by a finite small slope in the isotherm. This liquid state arises due to residual capillary attractions between spherocylinders favoring local alignment, and corresponds to the gentle increase observed in surface pressure. Furthermore, the isotherm shows that compression induces another state transition after the solid phase, where the slope of the isotherm decreases and the surface pressure steadily rises to higher values without collapse. From our own observations (see below) and by comparison with [15], we interpret this apparent transition as due to the combined effects of buckling, "flipping" and bilayer formation. Shorter particles (AR≃3, blue curve in Fig. 1) show no sign of a liquid state, and their isotherm resembles that of spherical particles, presumably due to weaker capillary attractions [23].

We next analyse the results of our microscopy studies (see SI for details). These images (Fig. 2) help us interpret the isotherm results, and provide more information about the series of state transitions discussed above. For AR≃3, our data are suggestive of at least two state transitions. For low surface coverage, the monolayer has not yet formed, and we observe isolated aggregates of particles (Fig. 2a, trough area = 80 cm$^2$, gas state): these are likely kept together by residual weak capillary interactions. As the area is decreased the aggregates form a percolating network, and when the density is sufficiently large we observe a uniform monolayer (Fig. 2b, trough area = 60 cm$^2$, solid state). As the density increases to approach random close packing, particles jam: here, further compression does not trigger any more in-plane particle rearrangement; instead, the monolayer buckles, forming folds perpendicular to the compression direction (visible as darker regions in Fig. 2c, trough area = 30 cm$^2$).

For spherocylinders with AR≃9 (Fig. 2d-f), at low surface coverage we observe that particles pair either end-to-end or side-to-side (Fig. S1) due to capillary interactions (Fig. 1, gas state). At higher density, an inhomogeneous monolayer forms (Fig. 2d, trough area = 80 cm$^2$, liquid state). Microscopy shows that, in this regime, dense rafts of jammed spherocylinders with local nematic ordering coexist with long-lived voids. Upon further compression, the voids shrink (Fig. 2e, trough area = 60 cm$^2$, solid state), and we observe particle flipping (Fig. 2f, trough area 30 cm$^2$). Flippers often form in clusters – some of these are highlighted in red in Fig. 2f. Even when flippers appear, some voids are surprisingly still present: this may be linked to the previous finding of an inhomogeneous compressive stress in an ellipsoid monolayer [15]. As for shorter spherocylinders (Fig. 2c), buckling eventually occurs also for AR≃9. Buckling is nucleated at the monolayer edges (Fig. S2), indicating that the compressional stress is stronger close to the approaching barriers.

Fig. S3 shows more images of compressed monolayers with AR≃9, comparing the microscopic features of the same field of view at trough area 50 cm$^2$ and 32 cm$^2$. Flipper clusters (highlighted in red) localise in regions with low nematic ordering, where they reduce particle coverage, which relieves compressional stress. These clusters are usually string-like, and perpendicular to the compression direction. Particles in more ordered domains seem to be on average less likely to flip (highlighted in green). Void regions have different shapes: some are irregular, others are triangular (highlighted in yellow and white, respectively): the latter are stable, presumably because their higher symmetry corresponds to a locally homogeneous compressional stress.

Spherocylinders with the largest AR, 15 (Figs. 2g-i), form a more open network at the interface, (Fig. 2g, trough area = 80 cm$^2$, close to the gas-liquid transition). Dynamic compression drives particle rearrangement, and a transition to a final state with locally ordered particle rafts (Figs. 2h,i, trough area 30 and 25 cm$^2$ respectively). This transition is superficially similar to the one described above, for AR≃9. There are some important differences though. First, the void regions and ordered

domains are much more stable and survive through to the end of the compression (highlighted in yellow and green in Fig. 2i, trough area 25 cm$^2$). Second, we observe no flipping for these longer spherocylinders. Instead, particles in dense and disordered regions appear to form a bilayer (Figs. 2h and 2i, highlighted in red). The formation of regular layers provides another route to relieving compressional stress, alternative to flipping.

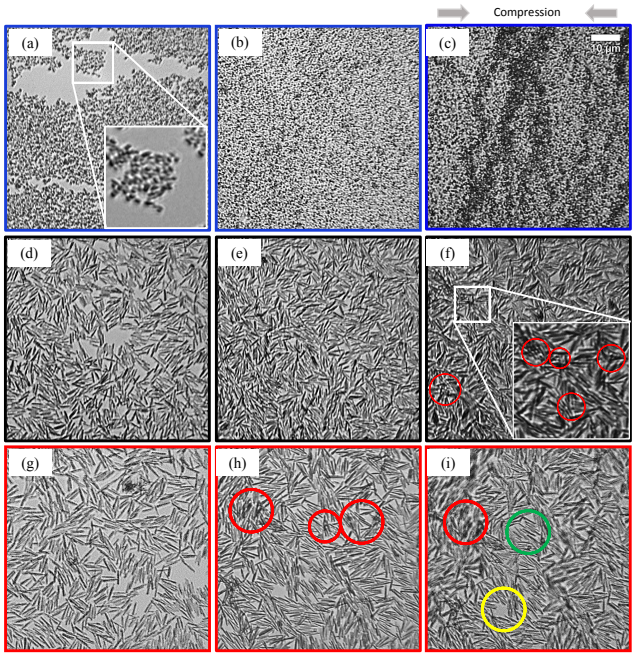


FIG. 2: Morphological transitions in compressed monolayers, observed via microscopy. (a-c) Rods with AR≃3. The trough area is 80 cm$^2$ (a), 60 cm$^2$ (b), 30 cm$^2$ (c), respectively. (d-f) Rods with AR≃9. The trough area is 80 cm$^2$ (d), 60 cm$^2$ (e), 30 cm$^2$ (f), respectively. Flippers are marked in red. (g-i) Rods with AR≃15. The trough area is 80 cm$^2$ (g), 30 cm$^2$ (h), and 25 cm$^2$ (i), respectively. Bilayer aggregates are marked in red; locally ordered structures in green, and voids in yellow. Scale bar = 10$\mu$m. The inset of (a) and (f) are zoomed-in views.

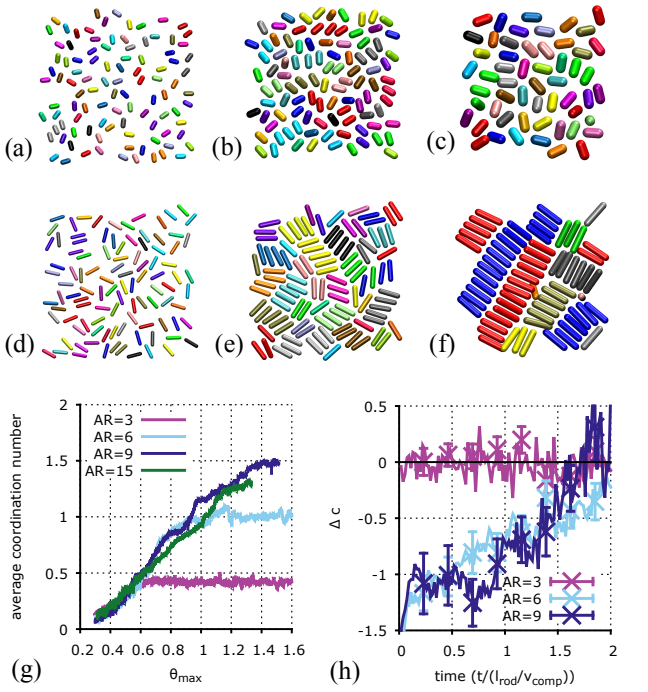


FIG. 3: Compression of rod monolayers with ARs 3 and 6 studied by DPD simulations. (a-c) Snapshots of the AR=3 monolayer at $\theta_{\max}$=0.3 (a), $\theta_{\max}$=0.7 (b), $\theta_{\max}$=1.4 (c). (d-f) Snapshots of the AR=6 monolayer at $\theta_{\max}$=0.3 (d), $\theta_{\max}$=0.7 (e), $\theta_{\max}$=1.4 (f). We can notice the "flipper" in panel f in pink. (g) Average coordination number (see text) versus $\theta_{\max}$ for different AR. (h) The differential order $\Delta C$ (see SI) versus time: flipping events are correlated with the local order for AR=6 and 9, but not for AR=3.

To understand our experiments more quantitatively, we performed computer simulations by dissipative particle dynamics (DPD, see SI for details); all simulations were performed using the program LAMMPS [18]. We modelled colloidal spherocylinders as rigid bodies, built from spherical beads, adsorbed on a flat water-oil interface, while water and oil molecules are modelled explicitly at a mesoscopic level as spherical beads of mass $m$ and effective radius $r_c$ interacting with a suitable force field (see SI). The surface tension of the interface in our simulations is $\gamma = 4.2\ k_BT/r_c^2$, which maps to $\sim 17$ mN/m for nanoparticles ($r_c \sim 1$nm). As in experiments, spherocylinders spontaneously cover the interface because by doing so they decrease the system free energy (Fig. S4).

We considered spherocylinders of ARs 3, 6, 9 and 15 – the corresponding adsorption energies are 25.4, 50.1, 69.8 and 119.2 $k_BT$ respectively: even if these are smaller than in experiments, they still lead to irreversible adsorption, unless under very high compaction (see SI for a discussion of the limitations of our simulations). In what follows, energy, length and time are expressed in units of $k_BT$, $r_c$, and $\tau = \sqrt{mr_c^2/(k_BT)}$ respectively. For each AR, we simulate dynamic compression by reducing the size of the simulation box along the $x$ and $y$ directions (at a constant speed $v_c = 0.0003 r_c/\tau$) while expanding it along $z$ to keep the volume constant; this is done in a system where water and oil are phase separated along $z$, with periodic boundary conditions along all three directions (so there are two interfaces in the simulation domain). We consider $N = 100$ spherocylinders initially adsorbed at one interface, with an initial surface coverage, $\theta$ (see SI), equal to 0.3. A convenient coordinate to describe the progression of compression is $\theta_{\max}$, which measures the theoretical maximal packing for a given trough area, computed assuming all particles lie on the interface keeping their optimal orientation parallel to it. For $\theta_{\max} > 1$, spherocylinders cannot form a single monolayer while re-

maining in this optimal configuration: they need to either desorb, flip, or form a bilayer.

We first discuss the simulation results for AR up to 9 (snapshots in Figs. 3a-c and 3d-f correspond to AR 3 and 6 respectively). For the shorter particles, compression leads to jamming, without appreciable nematic ordering; when $\theta_{\max}$ increases we also observe desorption (Fig. S5, and SI). The absence of orientational ordering is apparent from Fig. 3g, where the average coordination number within locally aligned domains is plotted versus time. This result explains the absence of the liquid state in the isotherms in Fig. 1 for the AR 3; it is further consistent with simulations of 2-dimensional rod-like particles which show an isotropic-to-nematic transition for AR close to 7 [19].

For AR=6, local nematic domains appear (Figs. 3e and 3f), in line with our observation of a liquid state in the isotherm (Fig. 1). Importantly, when increasing $\theta_{\max}$, desorption is much less frequent (Fig. S5) and before this occurs we observe flipping (Fig. 3f, Movie S1). Flipping is also found for AR=9, albeit at a smaller rate (Fig. 4c, Movie S2). We correlate the onset of flipping with the onset of non-zero global nematic order. Therefore, our simulations suggest that the four states observed in the isotherms in Fig. 1 for longer particles respectively correspond to: gas, liquid with local (nematic) order, solid with local order, solid with global order (with or without flipping).

Visual inspection of flipping events suggest these occur at the boundary between ordered domains, or equivalently in a locally disordered region. To quantify this, we identify all flippers, and compute the local orientational order around them. It is convenient to define the differential order $\Delta C$ (see SI), which is negative for rods having less local order than the average, and positive otherwise. We find $\Delta C$ just before flipping is negative for AR=6 or 9 (Fig. 3h). For shorter AR, there are no flippers but we can still track desorbing particles: these do not have a different local order, and $\Delta C \sim 0$ – reflecting the very weak nematic ordering in those monolayers.

We next examine our simulation results for the largest AR, 15. Here, flipping is absent (there is also no desorption, Fig. S5); the spherocylinders instead respond to compression by forming a bilayer, just as in our experiments (Fig. 4f). Fig. 4g shows that the effective surface coverage may exceed 1 (the largest possible in 2D), which signals bilayer formation; this phenomenon occurs for AR=15, and partially for AR=9, but not for AR$\leq$6. Pleasingly, therefore, in both simulations and experiments we find bilayer formation for particles with higher AR. It is important to determine which physical mechanism may underlie this phenomenon. A key clue is that bilayers are not observed with ellipsoidal particles, either in our simulations (Fig. S6), or in experiments (at least prior to buckling) [15]. At least for neutral wetting (90 degree contact angle at the interface, as for our

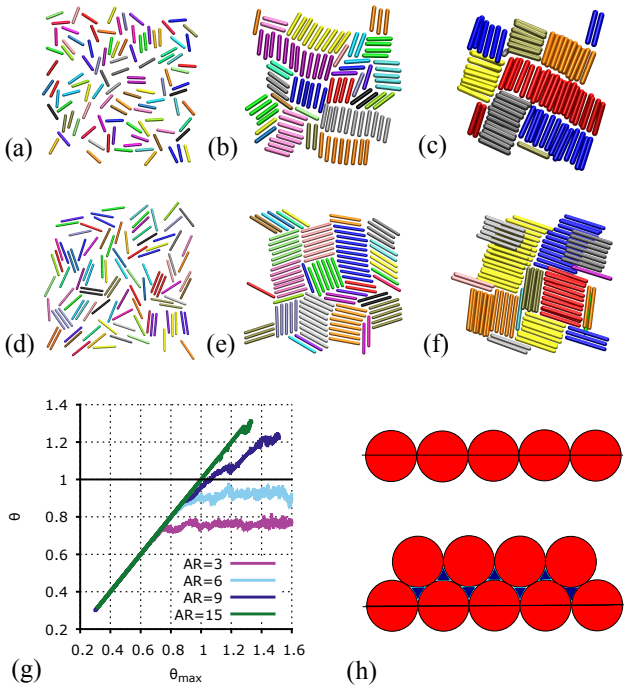


FIG. 4: Compression of rod monolayers with ARs 9 and 15 studied by DPD simulations. (a-c) Snapshots of the AR=9 monolayer at $\theta_{\max}$=0.3 (a), $\theta_{\max}$=0.7 (b), $\theta_{\max}$=1.4 (c). (d-f) Snapshots of the AR=15 monolayer at $\theta_{\max}$=0.3 (d), $\theta_{\max}$=0.7 (e), $\theta_{\max}$=1.3 (f). We note a "flipper" in (c) in grey and bilayer regions in (c,f). (g) Effective surface coverage $\theta$ (measured by assuming all adsorbed particles lie parallel to the interface) versus $\theta_{\max}$ for different ARs: $\theta > 1$ signals bilayer formation. (h) Schematics of the mechanism underlying bilayer formation: for wetting angle equal to 90 degrees, bilayer formation does not require any extra interfacial area.

DPD simulations), a possible reason is that ideal, infinitely long, spherocylinders can be arranged in a bilayer remaining in their optimal configuration parallel to the interface, without the creation of any extra interfacial area (Fig. 4h). This is not true for either ellipsoids or cylinders, which cannot fit snugly close to each other and also experience substantial capillary interactions favouring aggregation [12].

In summary, we studied the compression dynamics of a suspension of spherocylinders at an interface, by means of experiments and computer simulations. The response of spherocylinders depends strongly on their AR, as this quantity, together with packing density, determines the magnitude of local and global nematic ordering and the energetics of flipping. Short particles respond similarly to spherical particles, forming a uniform monolayer which buckles upon compression. Longer spherocylinders may respond by flipping their long axes perpendicular to the interface. By combining our microscopy observations and our simulations we elucidated the physics behind this previously elusive flipping: it occurs at regions where the

nematic ordering is low, or at boundaries between nematic domains. We have further shown that the longest particles display a qualitatively different phenomenon: upon compression the spherocylinders rearrange to form locally a bilayer structure. Bilayer formation is unique to the spherocylindrical geometry and is not observed, for instances, with ellipsoids. Besider uncovering new interfacial soft matter physics, our results provide a physical principle to design exotic Pickering emulsions and foams based on anisotropic colloids. We also expect that our self-assembling colloidal bilayers will provide a useful model system to study the physics of nematic shells with tunable thickness.

We acknowledge EPSRC (grant EP/J007404) for funding.

[1] S. Lam, K. P. Velikov, and O. D. Velev, Curr. Opin. Colloid Interface Sci. **19**, 490 (2014).
[2] P. Pieranski, Phys. Rev. Lett. **45**, 569 (1980).
[3] S. U. Pickering, J. Chem. Soc., Transactions **91**, 2001 (1907).
[4] L. Botto, E. P. Lewandowski, M. Cavallaro, and K. J. Stebe, Soft Matter **8**, 9957 (2012).
[5] S. C. Glotzer and M. J. Solomon, Nat. Mater. **6**, 557 (2007).
[6] R. G. Alargova, D. S. Warhadpande, V. N. Paunov, and O. D. Velev, Langmuir **20**, 10371 (2004).
[7] F. Gunther, S. Frijters, and J. Harting, Soft Matter **10**, 4977 (2014).
[8] B. Madivala, S. Vandebril, J. Fransaer, and J. Vermant, Soft Matter **5**, 1717 (2009).
[9] B. Madivala, J. Fransaer, and J. Vermant, Langmuir **25**, 2718 (2009).
[10] J. C. Loudet and B. Pouligny, EPL **85**, 28003 (2009).
[11] B. J. Newton and D. M. A. Buzza, Soft Matter **12**, 5285 (2016).
[12] L. Botto, L. Yao, R. L. Leheny, and K. J. Stebe, Soft Matter **8**, 4971 (2012).
[13] T. Li *et al.*, Langmuir **30**, 13854 (2014).
[14] F. Si, B. Li, W. Margolin, and S. X. Sun, Sci. Rep. **5**, 11367 (2015).
[15] M. G. Basavaraj, G. G. Fuller, J. Fransaer, and J. Vermant, Langmuir **22**, 6605 (2006).
[16] A. Maitra, P. Srivastava, M. Rao, and S. Ramaswamy, Phys. Rev. Lett. **112**, 258101 (2014).
[17] N. Hijnen and P. S. Clegg, Chem. Mater. **24**, 3449 (2012).
[18] S. Plimpton, J. Comput. Phys. **117**, 1 (1995).
[19] M. A. Bates and D. Frenkel, J. Chem. Phys **112**, 10034 (2000).
[20] J. T. Petkov and T. D. Gurkov, Langmuir **16**, 3703 (2000).
[21] T. Verwijlen, L. Imperiali, and J. Vermant, Advances in Colloid and Interface Science **206**, 428 (2014).
[22] In practice, imperfections in the fabrication processes mean that weak residual capillary interactions can still be present.
[23] We refrain from a more detailed interpretation of isotherms, as, especially for large compression, these require disentangling thermodynamic and mechanical contributions [20, 21].